Biomimetic Persistent Luminescent Nanoplatform for Autofluorescence-Free Metastasis Tracking and Chemo-photodynamic Therapy

Yu-Jie Li, Cheng-Xiong Yang, and Xiu-Ping Yan

Anal. Chem., **Just Accepted Manuscript** • DOI: 10.1021/acs.analchem.8b00311 • Publication Date (Web): 05 Mar 2018

Biomimetic Persistent Luminescent Nanoplatform for Autofluorescence-Free Metastasis Tracking and Chemo-photodynamic Therapy

Yu-Jie Li[†], Cheng-Xiong Yang[†] and Xiu-Ping Yan*[,†,‡,§]

[†] College of Chemistry, Research Center for Analytical Sciences, State Key Laboratory of Medicinal Chemical Biology, Tianjin Key Laboratory of Molecular Recognition and Biosensing, Nankai University, Tianjin 300071, China

[‡] State Key Laboratory of Food Science and Technology (Jiangnan University), Institute of Analytical Food Safety, School of Food Science and Technology, Jiangnan University, Wuxi 214122, China

[§]Collaborative Innovation Center of Chemical Science and Engineering (Tianjin), Tianjin 300071, China

* Fax: (86) 22 23506075. E-mail: xpyan@nankai.edu.cn；xpyan@jiangnan.edu.cn.

ABSTRACT: Metastasis is the main cause of death in people with cancer. Early diagnosis and targeted therapy for metastasis is crucial for the survival of the cancer patients. However, metastasis is hard to trace for its small size, dispersed distribution and unvascularized anatomy. Here we report a biomimetic persistent luminescent nanoplatform for non-invasive high-sensitive diagnosis and 808 nm laser controlled photodynamics assisted chemotherapy of metastasis. The nanoplatform is composed of a photosensitizer functionalized persistent luminescent nanoparticle core, a doxorubicin loaded hollow silica interlayer and a cancer cell membrane shell for effective metastasis theranostic. The cancer cell membrane shell prevents drug leakage and endows the nanoplatform with targeting ability to metastasis. The re-activatable persistent luminescence of persistent luminescent nanoparticles not only enables long term *in vivo* metastasis tracking, but also provides internal light source for singlet oxygen generation to kill cancer cells and further break the membrane shell for drug release. This work provides a promising strategy to develop persistent luminescence imaging guided theranostic nanoplatforms for early metastasis.

Metastases are the products of tumor development that involves dissemination of cancer cells to anatomically distant organ sites and subsequent adaptation to foreign tissue microenvironments.[1] Despite advanced and mature surgical resections can cure well confined primary tumors, metastasis is still hard-to-treat for its systemic nature.[2] As over 90% of cancer patients died from metastases rather than primary tumors, specific diagnosis and targeted therapy for metastasis is of urgent need.[1-3] Although a few excellent works on metastases therapy have been reported,[4-8] integrated precise diagnosis and controllable therapy for metastases has not been realized yet.

Optical imaging offers great advantages in disease diagnosis due to its high sensitivity, non-invasion and cost-effective nature.[9-11] However, traditional optical imaging probes are not suitable for metastasis imaging because the true signals of metastasis are scattered and weak, and easily masked by the autofluorescence background under real-time excitation due to their tiny size and distant desperation.[2,3] Persistent luminescent nanoparticles (PLNPs) are unique optical materials with long-lasting luminescence after stopping excitation. Such unique luminescent nature permits optical detection without external illumination to avoid tissue autofluorescence from *in situ* excitation.[12-16] Besides, PLNPs with NIR emission have additional advantages of deep penetration and persistent luminescent renewability by NIR light for bioimaging, long-term *in vivo* tracing and internal light induced photodynamic therapy,[17-21] being ideal materials to build theranostic nanoplatforms for metastases.

Nanoparticles based theranostic platforms have been widely used in primary tumor therapy based on vascularization dependent enhanced permeability and retention (EPR) effect.[22] However, the unvascularized metastasis largely inhibits the ERP induced passive targeting effects of the nanoparticles.[2] Furthermore, conventional active targeting ligands such as antibodies, peptides and aptamers[23] give limited specificity and binding affinity to metastases.[6] Consequently, new targeting protocols for metastases are of urgent need. Nowadays, biomimetic membrane based delivery systems have attracted much attention due to their excellent bio-stability and little drug-leak in physiological conditions.[5, 6, 24-27] The homotypic attachment effect of cancer cells provides inspirations to build biomimetic membrane based systems with cancer cell membrane for metastases targeting.[4, 5, 28]

Herein, we report a biomimetic persistent luminescent nanoplatform for autofluorescence-free tracking and 808 nm laser controlled chemophotodynamic therapy of metastasis. The nanoplatform consists of a silicon phthalocyanine (Si-Pc) functionalized PLNPs core (SPLNPs), a doxorubicin (DOX) loaded hollow silica interlayer ($hSiO_2$) and a cancer cell membrane (CCM) shell. The $hSiO_2$ endows the nanoplatform with

high drug loading capacity. The CCM shell not only inhibits premature drug leakage during blood circulation, but also gives prominent targeting ability for metastases. The renewable NIR afterglow of PLNPs enables long term autofluorescence-free metastases tracking and provides internal light source for singlet oxygen ($^1O_2$) generation from Si-Pc. The persistent luminescence-induced $^1O_2$ can not only accelerate the endosomal escape of the nanoplatform for intracellular drug release,[29] but also damage cancer cells to give synergistic photodynamics controlled chemophototherapy for metastases. This integrated nanoplatform provides guidance for precise controllable metastasis theranostics.

EXPERIMENTAL SECTION

Preparation of DSPLNPs@hSiO$_2$@CCM. PLNPs ($Zn_{1.25}Ga_{1.5}Ge_{0.25}O_4$:0.5%$Cr^{3+}$,2.5%$Yb^{3+}$, 0.25%$Er^{3+}$) were synthesized according to our previous work.[18] For further modifications, the acquired PLNPs were hydroxylated with NaOH aqueous solution (5 mM) under ultrasonic treatment for 3 h. To modify PLNPs with silicon Si-Pc, the synthesized PLNPs was firstly functionalized with γ-aminopropyltriethoxysilane (APTES) via a condensation reaction of APTES with the surface hydroxyl groups of the PLNPs. Then, the photosensitizer Si-Pc was covalently linked to the surface of PLNPs-NH_2 via a reaction between the NH_2 groups on the surface of the PLNPs and Cl atoms in the Si-Pc molecules.[19] 20 mg hydroxylated PLNPs was dispersed in DMF (8 mL) under sonication, to which APTES (80 μL) was added under stirring at 80 °C for 24 h. The resulting particles were collected by centrifugation, and washed with DMF and ethanol absolute sequentially to remove the unreacted APTES. The NH_2-PLNPs were dried under vacuum overnight. Thus, NH_2-PLNPs were obtained. To conjugate Si-Pc to NH_2-PLNPs, 200 μg mL^{-1} of Si-Pc (5 mL) was mixed with NH_2-PLNPs by sonication. Subsequently, the mixture was gently stirred at room temperature in the dark for 30 h. Finally, the resulting complex were centrifuged and washed with ethanol to remove the excess Si-Pc to acquire Si-Pc conjugated PLNPs (SPLNPs).

Hollow silica coated SPLNPs (SPLNPs@hSiO$_2$) were synthesized with micro-emulsion method.[30] 2 mg of synthesized SPLNPs was dispersed in 2.1 mL H_2O. The SPLNPs aqueous dispersion, 29.65 g of cyclohexane, 10 g of Triton X-100 and 8 mL of hexanol were mixed at room temperature. Then, TEOS was added to the mixture. Two hours later, 500 μL of aqueous ammonia (28~30 wt %) was introduced to initiate the hydrolysis of tetraethylorthosilicate (TEOS). After 6 h, 200 μL of ethanolic solution of APTS was added and stirred continuously for 24 h. The reaction temperature was kept at 20 ^oC. After the reaction, ethanol was added to destabilize the micro-emulsion system. The synthesized nanoparticles were isolated via centrifugation and washed with ethanol. At last, the product was soaked in water for 7 days to form the hollow spheres in SPLNPs@hSiO$_2$. The acquired complex was lyophilized to get dry SPLNPs@hSiO$_2$

To load SPLNPs@hSiO$_2$ with DOX, 20 mg prepared SPLNPs@hSiO$_2$ was dispersed in 25 mL DOX aqueous solution (0.08 mg mL^{-1}) for 24 h under magnetic stirring at room temperature. The final mixture was centrifuged and washed with PBS to remove the residual free DOX to acquire DOX loaded SPLNPs@hSiO$_2$ (DSPLNPs@hSiO$_2$). The supernatants were collected for UV-vis spectrophotometer to determine the loading and encapsulation efficiency of DOX.

The 4T1 cell membrane vesicles (CCM) were prepared according to a published method.[4] The 4T1 cells were harvested and treated with the Tris buffer (pH = 7.4) at 4 °C for 1 h, homogenized and centrifuged at 500 × g for 10 min to remove the intracellular contents. Then, the supernatants were centrifuged at 10,000 × g for 10 min and 100,000 × g for 1 h to get the cell pellets. The received pellets were washed with PBS, sonicated for 5 s using an ultrasonicator and extruded through 400 nm polycarbonate membranes for 4 times to obtain CCM.

To coat SPLNPs@hSiO$_2$ with CCM, the mixture of prepared SPLNPs@hSiO$_2$ and CCM were extruded through a 200 nm polycarbonate membranes for 4 cycles to give SPLNPs@hSiO$_2$@CCM. Similarly, to coat DSPLNPs@hSiO$_2$ with CCM, the mixture of prepared DSPLNPs@hSiO$_2$ and CCM were extruded through a 200 nm polycarbonate membranes for 4 cycles to obtain DSPLNPs@hSiO$_2$@CCM. To prepare UV light pre-irradiated DSPLNPs@hSiO$_2$@CCM, the prepared DSPLNPs@hSiO$_2$ was irradiated with 254 nm UV lamp for 10 min. The pre-excited DSPLNPs@hSiO$_2$ was then mixed with prepared CCM at 15 min post the cease of UV irradiation. The mixture of prepared DSPLNPs@hSiO$_2$ and CCM were extruded through a 200 nm polycarbonate membranes for 4 cycles to give UV light pre-irradiated DSPLNPs@hSiO$_2$@CCM. The UV light pre-irradiated SPLNPs@hSiO$_2$@CCM was synthesized in the same way.

Cell Culture and Animals. 4T1 cells were obtained from cell bank of Shanghai, Chinese Academy of Sciences. 4T1 cells were cultured and then expanded in a 10 cm^2 plate in the RPMI 1640 medium (Gibico, USA) supplemented with 10% fetal bovine serum and 100 U mL^{-1} of penicillin–streptomycin, 2.5 g L^{-1} glucose and 0.11 g L^{-1} sodium pyruvate at 37 °C in 5% CO_2.

Female Balb/c nude mice (4 week old, 18–22 g) were purchased from HFK Bioscience Co. (Beijing, China). The orthotopic 4T1 tumor model was established by subcutaneous injection of 4T1 cells into the mammary fat pad of female Balb/c mice. 4T1 cells were collected by trypsinization, washed and resuspended in PBS (5 × 10^5 cells in PBS). The cells were injected stereotactically to the second mammary fat pad on the left side of the mice. The mice were anesthetized with intraperitoneally administered pentobarbital in all animal procedures. All experiments for animals were performed under the instructions of the Tianjin Committee of Use and Care of Laboratory Animals.

***In Vivo* Background Free Metastasis Tracing.** *In vivo* bioimaging and distribution of DSPLNPs@hSiO$_2$, DSPLNPs@hSiO$_2$@LP and DSPLNPs@hSiO$_2$@CCM were determined in the orthotopic breast tumor model. The orthotopic 4T1 tumor model was established by subcutaneous injection of 6 × 10^5 4T1 cells into the second mammary fat pat of female Balb/c mice. After two weeks, the nude mice were randomly separated to three groups (3 mice in each group) and injected intravenously with 0.04 mg g^{-1} of UV light pre-irradiated DSPLNPs@hSiO$_2$@CCM, DSPLNPs@hSiO$_2$@LP or UV light pre-irradiated DSPLNPs@hSiO$_2$ (To prepare UV light pre-irradiated nanomaterials, the DSPLNPs@hSiO$_2$ was irradiated with 254 nm UV lamp for 10 min and separated into three groups. One group was coated with CCM at 15 min post

the cease of UV irradiation to give UV light pre-irradiated DSPLNPs@hSiO$_2$@CCM, one group was coated with lipsome at 15 min post the cease of UV irradiation to give UV light pre-irradiated DSPLNPs@hSiO$_2$@LP while the other group without any modifications was UV light pre-irradiated DSPLNPs@hSiO$_2$. The interval between the cease of UV irradiation and the intravenous injection was 20 min in all the tested groups). The mice were laid on their backs for *in vivo* bioluminescence signal acquisition. All luminescence images were taken on IVIS imaging system 1, 4, 8 and 24 h post injection. The mice were excited with the LED light (650 ± 10 nm 2000 lm) for 2 min to re-activate the persistent luminescence of DSPLNPs@hSiO$_2$@CCM at 8 h post injection. The bioluminescence acquisition time was set to 90 s, without any excitation and emission filters and excitation source.

To further investigate the *ex vivo* biodistribution of nanoparticles, the nude mice were randomly separated to three groups and injected intravenously (i.v.) with 0.04 mg g^{-1} of UV light pre-irradiated DSPLNPs@hSiO$_2$@CCM, DSPLNPs@hSiO$_2$@LP or UV light pre-irradiated DSPLNPs@hSiO$_2$. The mice were sacrificed at 1, 4, 8 and 24 h post injection for organ collection. The main organs (i.e. heart, liver, spleen, lung, kidney and tumor) were collected for luminescence imaging. After the imaging, the collected organs were digested in aqua regia for one week. The resulting solution was filtered and diluted. The content of PLNPs in the above solution was determined by ICP-MS for monitoring the biodistribution of the nanoplatforms.

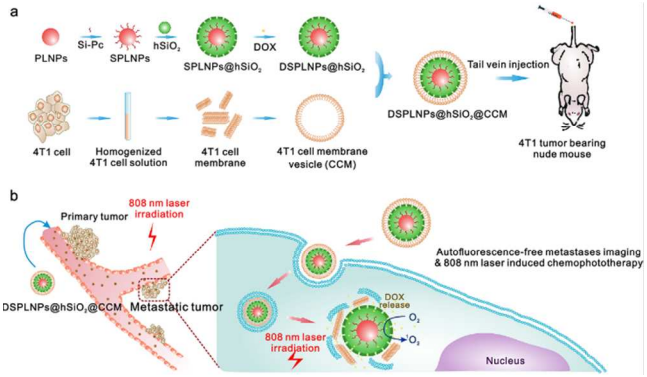

Scheme 1. Synthesis and application of DSPLNPs@hSiO$_2$@CCM. (a) Schematic representation of the design strategy and synthesis route. (b) *In vivo* background-free metastases imaging and 808 nm laser induced chemophototherapy.

RESULTS AND DISCUSSION

Preparation and Characterization of DSPLNPs@hSiO$_2$@CCM. The design and preparation of the biomimetic nanoplatform for non-invasive diagnosis and targeted therapy of metastasis is illustrated in Scheme 1a. Ultrabright monodispersed triple-doped zinc gallogermanate PLNPs (ZGGO:Cr^{3+},Yb^{3+},Er^{3+}) was prepared as the core of the nanoplatform based on our previous work due to its super-long and re-activatable (by red LED light or 808 nm laser) NIR persistent luminescence.[18] The photosensitizer Si-Pc was then functionalized on to the PLNPs to endow the nanoplatform with photodynamic therapeutic ability.[19] Hollow silica shell (hSiO$_2$) was coated on the Si-Pc functionalized PLNPs (SPLNPs) via micro-emulsion method[30] for high dose drug loading[31] and CCM supporting. The prepared hollow silica coated SPLNPs (SPLNPs@hSiO$_2$) was loaded with DOX (DSPLNPs@hSiO$_2$) to get tumor killing activity.[4] Finally, to inhibit premature drug leakage during blood circulation, improve the biocompatibility, prolong the blood-circulation time and achieve the active metastatic tumor-targeting ability, the DSPLNPs@hSiO$_2$ was encapsulated with the CCM extracted from highly metastatic 4T1 mammary cells via extruding[6] to get DSPLNPs@hSiO$_2$@CCM.

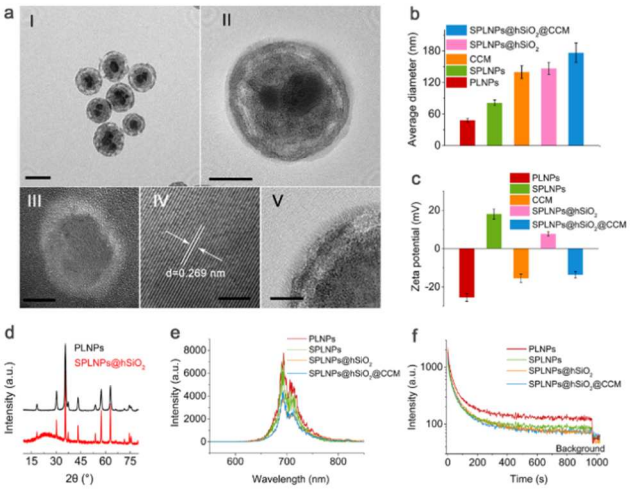

Figure 1. Characterization of SPLNPs@hSiO$_2$@CCM. (a) TEM images: (I) SPLNPs@hSiO$_2$ (scale bare 100 nm); (II,V) SPLNPs@hSiO$_2$@CCM (scale bar 50 and 20 nm respectively); (III) CCM (scale bar 50 nm); (IV) lattice structure of PLNPs (scale bar 5 nm). (b) Hydrodynamic diameters of PLNPs, SPLNPs, SPLNPS@hSiO$_2$, CCM and SPLNPs@hSiO$_2$@CCM measured by TEM. (c) Zeta potentials of PLNPs, SPLNPs, SPLNPS@hSiO$_2$, CCM and SPLNPs@hSiO$_2$@CCM. (d) XRD patterns of PLNPs and PLNPs@SiO$_2$. (e) Photoluminescence spectra of PLNPs, SPLNPs, SPLNPs@SiO$_2$ and SPLNPs@hSiO$_2$@CCM (λ_{ex}, 254 nm). (f) Persistent luminescence decay curves of PLNPs, SPLNPs, SPLNPs@SiO$_2$ and SPLNPs@hSiO$_2$@CCM (0.15 g each), monitored at 695 nm after 5 min 254 nm UV lamp irradiation. Data are given as mean ± s.d. (n = 5).

The prepared nanoplatform was characterized by transmission electron microscopy (TEM), Fourier transform infrared (FT-IR), Zeta potential analysis, dynamic light scattering, X-ray powder diffraction (XRD), N_2 adsorption and desorption test and fluorescence spectroscopy. The PLNPs core has the lattice space of 0.269 nm and the hydrodynamic diameter of 41.3 ± 5.6 nm before surface modification (Figure 1aIV and 1b). Functionalization with Si-Pc made the hydrodynamic diameter and the zeta-potential increase from 47.9 ± 3.6 nm to 81.3 ± 5.2 nm and from – 25.5 ± 2.0 mV to 18.1 ± 2.6 mV, respectively (Figure 1b and 1c). The appearance of the characteristic band for –N=C– at ~1631 nm^{-1} in the FT-IR spectra of SPLNPs confirms the successful conjugation of Si-Pc and PLNPs (Figure S1).[19] Coating of hSiO$_2$ on SPLNPs made the hydrodynamic diameter increase from 81.3 ± 5.2 nm to 146.5 ± 11.3 nm (Figure 1b), but the Zeta potential decrease from 18.1 ± 2.6 to 7.6 ± 1.3 mV due to the residual amino group on

the surface of the $hSiO_2$ shell (Figure 1c).[32] The new broad peak in the XRD pattern (Figure 1d), the TEM image (Figure 1aI), and the N_2 adsorption and desorption curve (Figure S2) of SPLNPs@$hSiO_2$ defined the hollow structure of coated $hSiO_2$.[30] SPLNPs@$hSiO_2$@CCM possessed a monodispersed core–shell structure (Figure 1aII) with the hydrodynamic diameter of 176.4 ± 18.7 nm (Table S1, Supporting Information) and Zeta potential of -13.7 ± 1.7 mV after CCM encapsulation. The encapsulated CCM shell has a thickness of ca. 10 nm (Figure 1aIII) and tuned the Zeta-potential from positive (7.6 ± 1.3 mV) to negative (-13.7 ± 1.7 mV) due to the negative charged CCM (-15.52 ± 3.18 mV) (Figure 1c). The minimal size increase of SPLNPs@$hSiO_2$@CCM throughout 24 h in diverse solutions indicates good colloidal stability of prepared persistent luminescent nanoplatform (Figure S3).

The PLNPs core has a NIR emission peak at 695 nm and super-long-lasting afterglow (more than 450 h) after 254 nm UV light excitation (Figure 1e; Figure S4). Importantly, the photoluminescence and persistent NIR luminescence of the PLNPs can be excited and re-activated with red LED and 808 nm laser irradiation via a photon-assisted excitation process (Figure S6-S9),[18,19,33] making it suitable for long-term autofluorescence free *in vivo* metastases imaging and 808 nm laser renewable persistent luminescence sensitized photodynamics assisted therapy. In a photon-assisted excitation process, the luminescence system was located in an intermediate state (above ground state, derived from thermal vibration) under thermal conditions (room temperature or higher). This intermediate state decreases the needed excitation energy of the second-step incident photons to excite the system to the excited states, which was confirmed by the 808 nm activated photoluminescence (Figure S9). The photoluminescence excitation, emission, afterglow intensity and renewable persistent luminescence of SPLNPs, SPLNPs@$hSiO_2$ and SPLNPs@$hSiO_2$@CCM do not change obviously in comparison with those of PLNPs (Figure 1e, 1f and Figure S5, S8).

Persistent Generation of $^1O_2$ without Continuous External Light Irradiation. The $^1O_2$ generation ability of SPLNPs@$hSiO_2$@CCM was evaluated by fluorescence quenching method with 1,4-diphenyl-2,3-benzofuran (DPBF).[19,34] The UV pre-excited SPLNPs@$hSiO_2$@CCM had neglect effect on the fluorescence of DPBF in the first 15 min as the attenuated persistent luminescence of PLNPs was not strong enough to excite the conjugated Si-Pc to generate adequate $^1O_2$ without *in situ* excitation. However, significant fluorescence quenching of DPBF occurred only in the presence of SPLNPs@$hSiO_2$@CCM along with 200 s irradiation with 808 nm laser (3.0 W cm^{-2}) owing to the re-activated photoluminescence and persistent luminescence of the PLNPs (Figure S10), confirming 808 nm laser irradiation for 200 s enables the regeneration of $^1O_2$ for photodynamic therapy without continuous *in situ* activation.

Persistent Luminescence Induced-Photodynamics Assisted Drug Release. The persistent $^1O_2$ generation capability of SPLNPs@$hSiO_2$@CCM also enables photodynamics assisted drug release for chemotherapy. The DOX loading and encapsulation efficiency of DSPLNPs@$hSiO_2$@CCM were 7.3 ± 0.4 % and 92.6 ± 0.5 %, respectively. The *in vitro* DOX release behavior was evaluated in 1640 medium (Figure S11). The DOX release dropped from 47.6 ± 5.5 % (DSPLNPs@$hSiO_2$) to 17.5 ± 2.9 % (DSPLNPs@$hSiO_2$@CCM) in the first 8 h as the CCM acted as a diffusion barrier for drug diffusion. This inhibition of drug release by the CCM shell significantly avoids drug leakage during blood circulation. 808 nm laser irradiation (3.0 W cm^{-2}) for 200 s significantly accelerated the DOX release from DSPLNPs@$hSiO_2$@CCM to 46.1 ± 4.6 % as the generated $^1O_2$ upon 808 nm laser irradiation remarkably disrupt the CCM layer of DSPLNPs@$hSiO_2$@CCM for DOX diffusion,[29] making it possible for photodynamics controlled drug release for chemotherapy.

Cellular Internalization and *In Vitro* 808 nm Laser Controlled Photochemotoxity. The stability of the CCM covered SPLNPs@$hSiO_2$@CCM was confirmed firstly by studying the cellular uptake of DiO labeled SPLNPs@$hSiO_2$@CCM (the CCM was stained with green light emitting DiO). After co-incubation with 4T1 cell, both of the SPLNPs@$hSiO_2$ (red) and CCM (green) existed around the cell nucleus and the fluorescent signals overlapped well with each other, indicating the CCM covered SPLNPs@$hSiO_2$@CCM is stable even upon cellular endocytosis (Figure S12).

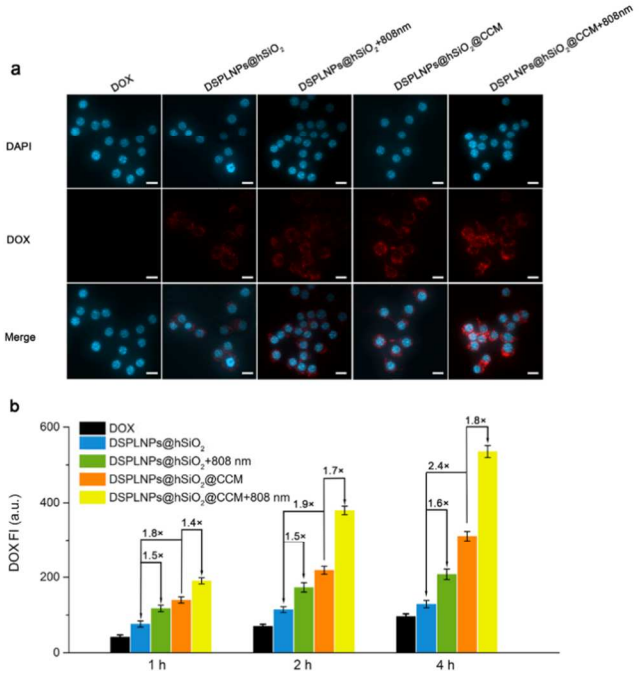

Figure 2. Cellular uptake assay. (a) Cellular internalization of the nanoparticles in 4T1 cells after 4 h incubation (scale bar 20 μm). (b) Intracellular fluorescence intensity of DOX. Data are given as the mean ± s.d. (n = 4)

Cellular internalization of DSPLNPs@$hSiO_2$@CCM was evaluated on 4T1 cells to verify its targeting ability to the cancer cells (Figure 2a). DSPLNPs@$hSiO_2$@CCM showed much brighter fluorescence of DOX in cytoplasm than DSPLNPs@$hSiO_2$, indicating the CCM shell remarkably accelerated the cellular uptake of DSPLNPs@$hSiO_2$@CCM as the retained cell membrane proteins on CCM remained the homotypic targeting ability of 4T1 cells.[28] After irradiation with 808 nm laser (3.0W cm^{-2}) for 200 s, DSPLNPs@$hSiO_2$@CCM gave a significant increase in the

fluorescence of DOX as the generated $^1O_2$ upon 808 nm laser irradiation remarkably disrupt the CCM layer of DSPLNPs@hSiO$_2$@CCM to speed up the diffusion of DOX and also accelerated the cellular uptake of the nanoparticle due to the increase of the cell membrane penetrability.[29]

The *in vitro* targeting effect of DSPLNPs@hSiO$_2$@CCM was quantified by flow cytometry assay (Figure 2b). The fluorescence intensity of DOX increased with time in all cases studied. DSPLNPs@hSiO$_2$@CCM gave stronger fluorescence intensity of DOX than DSPLNPs@hSiO$_2$ due to the CCM shell accelerated cellular internalization of DSPLNPs@hSiO$_2$@CCM to 4T1 cells. Additional 808 nm laser irradiation led to about 1.4, 1.7 and 1.8-fold increase of the fluorescence intensity of DOX in DSPLNPs@hSiO$_2$@CCM after incubation with 4T1 cells for 1, 2 and 4 h, respectively. DSPLNPs@hSiO$_2$@CCM with 808 nm laser irradiation exhibited the highest intracellular fluorescence intensity of DOX.

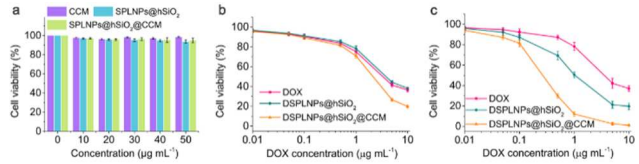

Figure 3. *In vitro* cytotoxicity assay. (a) *In vitro* cytotoxicity of CCM, SPLNPs@hSiO$_2$ and SPLNPs@hSiO$_2$@CCM. (b) *In vitro* dark cytotoxicity of DOX, DSPLNPs@hSiO$_2$ and DSPLNPs@hSiO$_2$@CCM. (c) Cytotoxicity of DOX, DSPLNPs@hSiO$_2$ and DSPLNPs@hSiO$_2$@CCM after irradiated with 808 nm laser for 200s. Data were obtained after 48 h incubation with 4T1 cells and given as the mean ± s.d. (n = 5).

The photodynamics controlled cytotoxicity of DSPLNPs@hSiO$_2$@CCM was evaluated on 4T1 cells. CCM, SPLNPs@hSiO$_2$ and SPLNPs@hSiO$_2$@CCM up to 50 μg mL^{-1} showed neglected cytotoxicity, indicating the good biocompatibility of the carriers (Figure 3a and Figure S13). The DSPLNPs@hSiO$_2$@CCM gave stronger cytotoxicity (IC_{50} 2.1 μg mL^{-1}) against 4T1 cells than DSPLNPs@hSiO$_2$ (IC_{50} 3.3 μg mL^{-1}) and DOX (IC_{50} 3.8 μg mL^{-1}) (Figure 3b) due to CCM layer accelerated cellular uptake of DSPLNPs@hSiO$_2$@CCM.[4, 6] Irradiation with 808 nm laser (3.0 W cm^{-2}) for 200 s did not affect the cytotoxicity of the free DOX, but increased the cytotoxicity of DSPLNPs@hSiO$_2$ by 3.3 times (IC_{50} 3.3 to 1.0 μg mL^{-1}), and DSPLNPs@hSiO$_2$@CCM by 7.9 times (IC_{50} 2.1 to 0.3 μg mL^{-1}) compared to no irradiation groups (Figure 3b and 3c). The enhancement of the cytotoxicity of DSPLNPs@hSiO$_2$ upon laser irradiation resulted from the phototoxiciy of Si-Pc. DSPLNPs@hSiO$_2$@CCM with 808 nm laser irradiation possessed the best anti-proliferative effects in the materials studied, as the CCM layer enhanced the uptake of DSPLNPs@hSiO$_2$@CCM to 4T1 cancer cells and can be destroyed by the 808 nm laser induced $^1O_2$ for enhanced drug release after entering the targeted cells, thus achieving synergistic efficacy of photodynamics controlled chemotherapy and photodynamic therapy against 4T1 cancer cells.

***In Vivo* Background-Free Metastases Tracing.** We then studied the targeting efficacy of DSPLNPs@hSiO$_2$@CCM to metastases *in vivo*. To this end, 4T1 cells were implanted in the left mammary fat pad of nude mice. *In vivo* targeted imaging for metastases with DSPLNPs@hSiO$_2$@CCM was conducted two weeks after tumor implantation (Figure 4 and Figure S17), as the highly aggressive 4T1 cells disseminated out of the primary tumor and colonized in the lung. The discrete tumor clusters rather than consecutive tumor tissues in the lung indicate the formation of pulmonary metastases rather than the local invasions of the left primary tumors (Figure S18). The UV lamp pre-irradiated DSPLNPs@hSiO$_2$@CCM was intravenously injected to 4T1 tumor bearing nude mice (0.04 mg g^{-1}). *In vivo* persistent luminescence images of the mouse show noticeable luminescence signals of DSPLNPs@hSiO$_2$@CCM on liver and primary tumor 1 h post injection due to the recognition of the reticuloendothelial system, the EPR effect of primary tumor and the active targeting effect of DSPLNPs@hSiO$_2$@CCM (Figure 4a and Figure S17). The autofluorescence background of mouse body was effectively eliminated during detection due to the absence of *in situ* excitation.[17] Although the intensity of persistent luminescence signals of DSPLNPs@hSiO$_2$@CCM on liver and primary tumor decreased with time without *in situ* excitation, new signals on metastases at lung was observed at 4 h post injection, indicating the metastatic targeting ability of DSPLNPs@hSiO$_2$@CCM (Figure 4a and Figure S17).

To further demonstrate the targeting ability of DSPLNPs@hSiO$_2$@CCM to the metastases, long-term background-free real-time imaging was conducted by taking advantage of the renewable ability of the PLNPs with red LED light irradiation.[18] 2-min red LED light reactivation of DSPLNPs@hSiO$_2$@CCM was carried out at 8 h post injection *in vivo* (Figure 4a, 4b and Figure S17). The intensity of the luminescence signal was significantly enhanced after reactivation. The signal intensity increased with time at metastases (lung site) (Figure 4a and Figure S17). However, the head to head comparison test with DSPLNPs@hSiO$_2$ and lipsome covered nanoplatform DSPLNPs@hSiO$_2$@LP only revealed luminescence signals on liver and primary tumor under the same detection conditions, indicating the intravenously injected DSPLNPs@hSiO$_2$ and DSPLNPs@hSiO$_2$@LP only had targeting ability for primary tumors (Figure 4a and Figure S17).

The advantage of DSPLNPs@hSiO$_2$@CCM for autofluorescence-free tracking of metastasis over traditional fluorescence probes was proved by the parallel experiment with NIR dye (710 nm emission) loaded nanoparticle BODIPY@hSiO$_2$@CCM (Figure S14). Despite the dye loaded particle possessed higher fluorescence intensity over DSPLNPs@hSiO$_2$@CCM 24 h post intravenous injection, DSPLNPs@hSiO$_2$@CCM gave much higher SNR (53) than BODIPY@hSiO$_2$@CCM (2.7). Compared with the manifest persistent luminescence signals of DSPLNPs@hSiO$_2$@CCM in solid and metastatic tumor site (Figure 4a and Figure S17), the fluorescence signals for metastasis of the dye-loaded nanoparticles are covered by the overwhelming autofluorescence background (Figure S14), confirming the advantage of DSPLNPs@hSiO$_2$@CCM for high SNR metastasis tracking. Furthermore, the blank control with DSPLNPs@hSiO$_2$@CCM and DSPLNPs@hSiO$_2$ injected healthy mice revealed luminescence signals only on liver after long time circulation due to the reticuloendothelial uptake,[17] indicating the signals in the lung of the tumor bearing mouse

derive from the metastasis tracking effect of the nanoparticles rather than the nanoparticle aggregation.

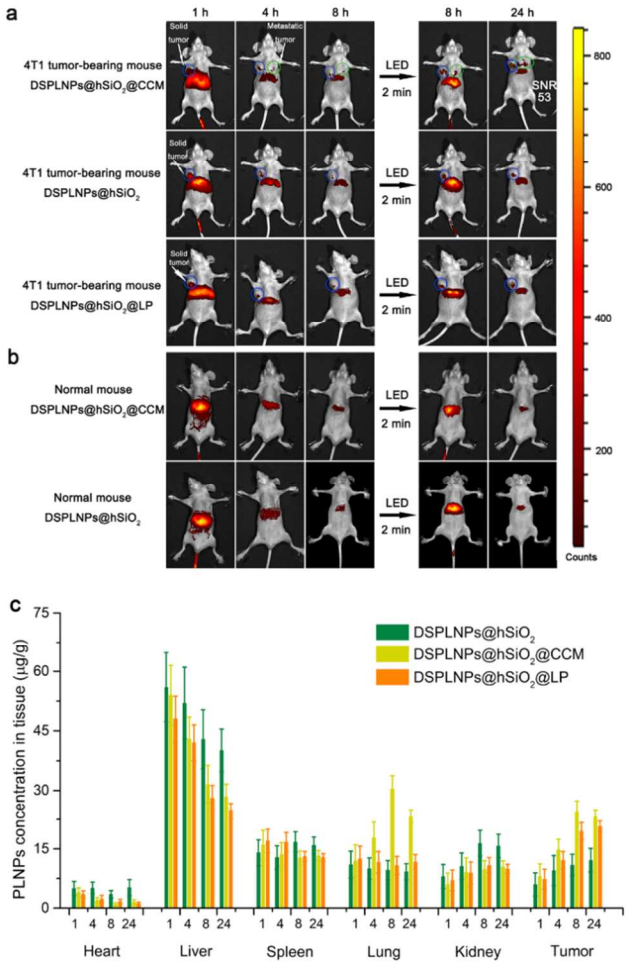

Figure 4. DSPLNPs@hSiO$_2$@CCM for *in vivo* autofluorescence-free metastatic 4T1 tumor imaging. (a) *In vivo* luminescence images of 4T1 tumor-bearing nude mice taken at different time points post i.v. injection of DSPLNPs@hSiO$_2$, DSPLNPs@hSiO$_2$@LP and DSPLNPs@hSiO$_2$@CCM (Blue circles locate the primary tumor site and green circles locate the metastatic tumor site). (b) *In vivo* luminescence images of normal nude mice taken at different time points post intravenous injection of DSPLNPs@hSiO$_2$ and DSPLNPs@hSiO$_2$@CCM. (c) Concentration of PLNPs in the main organs of the 4T1-breast-tumor-bearing mice at 1, 4, 8 and 24 h post intravenous injection of DSPLNPs@hSiO$_2$, DSPLNPs@hSiO$_2$@LP and DSPLNPs@hSiO$_2$@CCM. All the nanomaterials were UV pre-excited before intravenous injection. To prepare UV light pre-irradiated nanomaterials, the DSPLNPs@hSiO$_2$ was irradiated with 254 nm UV lamp for 10 min and separated into three groups. One group was coated with CCM at 15 min post the cease of UV irradiation to give UV light pre-irradiated DSPLNPs@hSiO$_2$@CCM, one group was coated with lipsome at 15 min post the cease of UV irradiation to give UV light pre-irradiated DSPLNPs@hSiO$_2$@LP while the other group without any modifications was UV light pre-irradiated DSPLNPs@hSiO$_2$. The interval between the cease of UV irradiation and the intravenous injection was 20 min in all the tested groups. Data are given as the mean ± s.d. (n = 5).

The *ex vivo* imaging of collected organs (24 h post intravenous injection) (Figure S15) reveal that only DSPLNPs@hSiO$_2$@CCM gave noticeable luminescence signal in both solid and metastases in the lung site. To further investigate the targeted accumulation of the CCM-coated nanoparticle in metastasis, the lungs collected in biodistribution assay were sectioned and observed on inverted fluorescence microscope (Figure S16). Strong red luminescence signals of PLNPs core were found at metastatic node in DSPLNPs@hSiO$_2$@CCM group, while only weak luminescence signals existed at the lung site in DSPLNPs@hSiO$_2$ and DSPLNPs@hSiO$_2$@LP group, indicating the specific accumulation of CCM-coated nanoparticle in the metastasis due to the increased interaction and uptake on metastatic cancer cells. These results confirm that the CCM layer significantly accelerated the targeting ability of DSPLNPs@hSiO2@CCM for lung metastasis compared to naked and lipsome covered materials (DSPLNPs@hSiO$_2$ and DSPLNPs@hSiO$_2$@LP).

The contents of DSPLNPs@hSiO$_2$, DSPLNPs@hSiO$_2$@LP and DSPLNPs@hSiO$_2$@CCM in the main organs of the 4T1-tumor-bearing mice were measured at 1, 4, 8 and 24 h post intravenous injection to assess their biodistribution (Figure 4c). Both of the three nanoplatforms distributed in the tested organs 1 h post injection, and mainly accumulated in liver and spleen in the first 4 h. The DSPLNPs@hSiO$_2$@CCM concentration in primary tumor was 2.1 and 1.2-fold higher than that of DSPLNPs@hSiO$_2$ and DSPLNPs@hSiO$_2$@LP at 8 h post injection. This superiority always existed until 24 h post injection. Furthermore, the accumulation of DSPLNPs@hSiO$_2$@CCM was remarkably superior to that of DSPLNPs@hSiO$_2$ in the lung (1.1, 1.8, 3.1 and 2.5-fold higher at 1, 4, 8 and 24 h post injection, respectively) and DSPLNPs@hSiO$_2$@LP in the lung (1.0, 1.5, 2.7 and 2.1-fold higher at 1, 4, 8 and 24 h post injection, respectively). The quantitative measurements indicate that DSPLNPs@hSiO$_2$@CCM accumulate in primary tumors and the metastases of lung with higher effectiveness than DSPLNPs@hSiO$_2$, in good agreement with the in vivo luminescence imaging measurements (Figure 4a, Figure S15 and Figure S17).

***In Vivo* 808 nm Laser Controlled Chemophotodynamic Therapy for Metastases.** The anti-metastases efficiency of DSPLNPs@hSiO$_2$@CCM was evaluated by counting the pulmonary metastatic nodules on the lungs of the 4T1 tumor-bearing mice (Figure 5a and 5d). H&E image shows lesions appeared in the lung 4 days post tumor implantation, indicating the formation of metastasis before therapy (Figure S19). The saline, SPLNPs@hSiO$_2$ and SPLNPs@hSiO$_2$@CCM group had the largest number of lung metastatic nodules (ca. 48 ± 7.1, 47 ± 3.7 and 45 ± 5.6 respectively). In contrast, the metastatic nodules in free DOX and DSPLNPs@hSiO$_2$@CCM group dropped to ca. 30 ± 4.0 and 16 ± 1.8 due to the lethality of the loaded DOX. DSPLNPs@hSiO$_2$@CCM gave better anti-metastasis effect (metastatic nodule 16 ± 1.8) than DOX (metastatic nodule 30 ± 4.0) due to CCM layer accelerated cellular uptake of DSPLNPs@hSiO$_2$@CCM (Figure 3b). 808 nm laser irradiation gave the best anti-metastasis effect of DSPLNPs@hSiO$_2$@CCM (metastatic nodule 2.0 ± 1.6) (Figure 5a and 5d), due to the active targeting effect of CCM layer, the phototoxicity of Si-Pc and the synergistic effect of the

accelerated DOX release from DSPLNPs@hSiO$_2$@CCM by laser induced $^1O_2$.

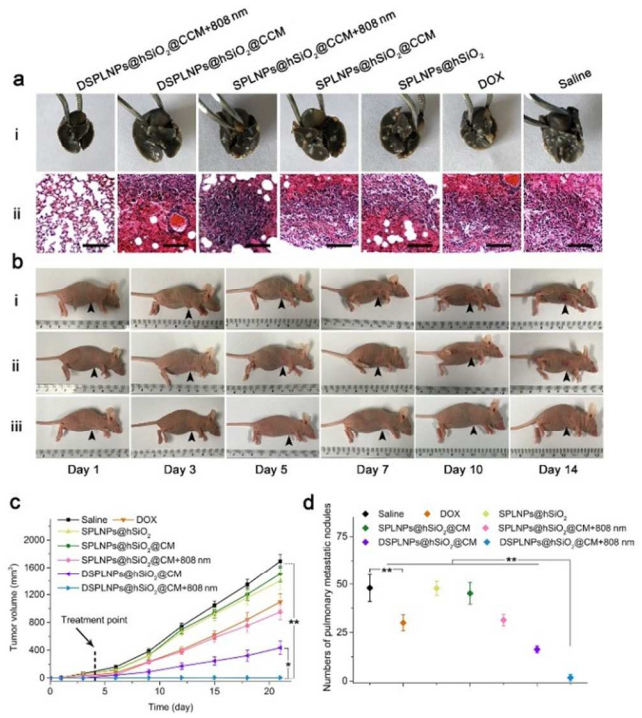

Figure 5. *In vivo* anti primary and metastases tumor effects of the DSPLNPs@hSiO$_2$@CCM in 4T1 tumor-bearing nude mice. (a) i, Collected lungs from the mice treated with saline, DOX, SPLNPs@hSiO$_2$, SPLNPs@hSiO$_2$@CCM, SPLNPs@hSiO$_2$@CCM with 808 nm laser irradiation, DSPLNPs@hSiO$_2$@CCM, and DSPLNPs@hSiO$_2$@CCM with 808 nm laser irradiation. ii, H&E staining of the lung tissues in Figure 5a(i) (scale bar 100 μm). The collected lungs were immersed in formalin for 7 days for specimen fixation before photographing and H&E staining. The raised white bumps on the lungs represent the sites of metastases. (b) Representative photographs of 4T1-tumor-bearing mice after treatment with i, saline, ii, DOX and iii, DSPLNPs@hSiO$_2$@CCM with 808 nm laser irradiation. The black arrows point to the injected tumor sites. (c) Tumor-growth profiles (the black arrow indicates the treatment point) and (D) quantitative analysis of pulmonary metastatic nodules for each group. All the nanoparticles of SPLNPs@hSiO$_2$, SPLNPs@hSiO$_2$@CCM and DSPLNPs@hSiO$_2$@CCM were UV light pre-excited before intravenous injection. For the 808 nm laser irradiation group, the metastases parts of the mouse were irradiated with 808 nm laser (3.0 W cm^{-2}) for 200 s after 4 h blood circulation of the nanoparticles intravenously injected to the mouse under the guidance of bioimaging. Data are shown as mean ± s.d. (n = 5). Statistical significance: *p < 0.05, **p < 0.005.

We also tested the ability of DSPLNPs@hSiO$_2$@CCM for anti-primary tumor in the orthotopic mammary tumor metastasis model (Figure 5b and 5c). The mice treated with saline, SPLNPs@hSiO$_2$ and SPLNPs@hSiO$_2$@CCM gave a rapid tumor growth as these drug-free materials did not have anti-tumor effect. The growth of the primary tumors slowed down obviously in the DOX and DSPLNPs@hSiO$_2$@CCM group and was completely inhibited in DSPLNPs@hSiO$_2$@CCM with 808 nm laser irradiation group (with a tumor inhibition rate of 99% compared with the saline injected group), indicating chemophototherapy is a promising emerging modality for treating solid tumors.[35] The negligibly weight change of the mice indicated low systemic toxicity of the nanoplatform (Figure S20). Furthermore, the histopathological measurements were also conducted on normal mice to evaluate the biosafety of the nanoparticles (Figure S21). Only the DOX group had weak inflammation in the heart and liver. The DSPLNPs@hSiO$_2$@CCM did not cause pathological changes in organs whether with NIR irradiation or not, indicating good biocompatibility of DSPLNPs@hSiO$_2$@CCM.

CONCLUSIONS

In conclusion, we have developed a new multiple functional persistent luminescent nanoplatform for precise metastasis theranostic. The nanoplatform is composed of a photosensitizer functionalized persistent luminescent nanoparticle core, a DOX loaded hollow silica interlayer and a cancer cell membrane shell for effective metastases theranostics. We have introduced cancer cell membrane shell to the nanoplatform to avoid drug leakage and endow the nanoplatform with targeting ability for metastases. The autofluorescence-free metastases tracing have been realized by taking advantage of the NIR light reactivatable character of PLNPs. The 808 nm laser renewable NIR persistent luminescence of PLNPs provides an internal light source for $^1O_2$ generation from PLNPs conjugated Si-Pc. The generated $^1O_2$ not only damage cancer cells, but also accelerate the endosomal escape of the nanoplatform for intracellular drug release to give synergistic photodynamics controlled chemophototherapy for metastases. We overcame the auto-fluorescence and realized precise controllable metastasis theranostics under optical imaging guidance with an integrated persistent luminescent nanoplatform. This accurate diagnose and controllable synergetic therapy for metastasis has not been realized before. This work provides a promising strategy to design precise and controllable drug delivery systems for metastases theranostics.

ASSOCIATED CONTENT

Supporting Information

The Supporting Information is available free of charge on the ACS Publications website.

Additional data of chemicals and materials, preparation of lipsome covered persistent luminescent nanoplatform (DSPLNPs@hSiO$_2$@LP), preparation of dye loaded nanoplatform (BODIPY@hSiO$_2$@CCM), colloidal stability of SPLNPs@hSiO$_2$@CCM, characterizations, Singlet oxygen ($^1O_2$) detection, DOX loading and release measurement, intracellular intergrity of SPLNPs@hSiO$_2$@CCM, cellular internalization assay, *in vitro* cytotoxicity and phototoxicity assay, *in vivo* bioimaging and biodistribution assay, *in vivo* comparison of DSPLNPs@hSiO$_2$@CCM with dye loaded nanoparticle BODIPY@hSiO$_2$@CCM, *in vivo* therapeutic effects for primary and metastatic tumors, *in vivo* biosafety assessment (PDF)

AUTHOR INFORMATION

Corresponding Author

* Fax: (86) 22 23506075. E-mail: xpyan@nankai.edu.cn; xpyan@jiangnan.edu.cn.

Notes

The authors declare no competing financial interest.

ACKNOWLEDGMENT

This work was supported by the National Natural Science Foundation of China (grant 21435001), the National Basic Research Program of China (2015CB932001) the Fundamental Research Funds for Central Universities (JUSRP51714B), and Open Funds of the State Key Laboratory of Electroanalytical Chemistry (SKLEAC201705).

REFERENCES

(1) Valastyan, S.; Weinberg, R. A. *Cell* **2011**, 147, 275-292.
(2) Schroeder, A.; Heller, D. A.; Winslow, M. M.; Dahlman, J. E.; Pratt, G. W.; Langer, R.; Jacks, T.; Anderson, D. G. *Nat. Rev. Cancer* **2012**, 12, 39-50.
(3) Chaffer, C. L.; Weinberg, R. A. *Science* **2011**, 331, 1559-1564.
(4) Sun, H. P.; Su, J. H.; Meng, Q. S.; Yin, Q.; Chen, L. L.; Gu, W. W.; Zhang, Z. W.; Yu, H. Z.; Zhang, P. C.; Wang, S. L.; Li, Y. P. *Adv. Funct. Mater.* **2017**, 27, 1604300.
(5) Rao, L.; Bu, L. L.; Cai, B.; Xu, J. H.; Li, A.; Zhang, W. F.; Sun, Z. J.; Guo, S. S.; Liu, W.; Wang, T. H.; Zhao, X. Z. *Adv. Mater.* **2016**, 28, 3460-3466.
(6) Sun, H. P.; Su, J. H.; Meng, Q. S.; Yin, Q.; Chen, L. L.; Gu, W. W.; Zhang, Z. W.; Yu, H. Z.; Zhang, P. C.; Wang, S. L.; Li, Y. P. *Adv. Mater.* **2016**, 9581-9588.
(7) Toledano Furman, N. E.; Lupu-Haber, Y.; Bronshtein, T.; Kaneti, L.; Letko, N.; Weinstein, E.; Baruch, L.; Machluf, M. *Nano Lett.* **2013**, 13, 3248-3255.
(8) Parodi, A.; Quattrocchi, N.; van de Ven, A. L.; Chiappini, C.; Evangelopoulos, M.; Martinez, J. O.; Brown, B. S.; Khaled, S. Z.; Yazdi, I. K.; Enzo, M. V.; Isenhart, L.; Ferrari, M.; Tasciotti, E. *Nat. Nano.* **2013**, 8, 61-68.
(9) Weissleder, R.; Pittet, M. J. *Nature* **2008**, 452, 580-589.
(10) Louie, A. Y. *Chem. Rev.* **2010**, 110, 3146-3195.
(11) Hellebust, A.; Richards-Kortum, R. *Nanomedicine* **2012**, 7, 429-445.
(12) de Chermont, Q. l. M.; Chaneac, C.; Seguin, J.; Pelle, F.; Maitrejean, S.; Jolivet, J.-P.; Gourier, D.; Bessodes, M.; Scherman, D. *Proc. Natl Acad. Sci. USA* **2007**, 104, 9266-9271.
(13) Pan, Z.; Lu, Y.-Y.; Liu, F. *Nat. Mater.* **2012**, 11, 58-63.
(14) Abdukayum, A.; Chen, J.-T.; Zhao, Q.; Yan, X.-P. *J. Am. Chem. Soc.* **2013**, 135, 14125-14133.
(15) Li, Y.; Gecevicius, M.; Qiu, J. *Chem. Soc. Rev.* **2016**, 45, 2090-2136.
(16) Wu, B.-Y.; Yan, X.-P. *Chem. Commun.* **2015**, 51, 3903-3906.
(17) Maldiney, T.; Bessière, A.; Seguin, J.; Teston, E.; Sharma, S.K.; Viana, B.; Bos, A.J.J.; Dorenbos, P.; Bessodes, M.; Gourier, D.; Scherman, D.; Richard, C. *Nat. Mater.* **2014**, 13, 418-426.
(18) Li, Y.-J.; Yan, X.-P. *Nanoscale* **2016**, 8, 14965-14970.
(19) Abdurahman, R.; Yang, C.-X.; Yan, X.-P. *Chem. Commun.* **2016**, 52, 13303-13306.
(20) Awuah, S.G.; Zheng, Y.-R.; Bruno, P. M.; Hemann, M. T.; Lippard, S. J. *J. Am. Chem. Soc.* **2015**, 137, 14854–14857.
(21) Xu, J. T.; Yang, P. P.; Sun, M. D.; Bi, H. T.; Liu, B.; Yang, D.; Gai, S. L.; He, F.; Lin, Jun. *Acs Nano* **2017**, 11, 4133-4144.
(22) Chen, G.; Roy, I.; Yang, C.; Prasad, P.N. *Chem. Rev.* **2016**, 116, 2826-2885.
(23) Chinen, A.B.; Guan, C.M.; Ferrer, J.R.; Barnaby, S.N.; Merkel, T.J.; Mirkin, C.A. *Chem. Rev.* **2015**, 115, 10530-10574.
(24) Hu, C.M.J.; Zhang, L.; Aryal, S.; Cheung, C.; Fang, R.H.; Zhang, L.F. *Proc. Natl Acad. Sci. USA* **2011**, 108, 10980-10985.
(25) Hu, C.-M.J.; Fang, R.H.; Wang, K.-C.; Luk, B.T.; Thamphiwatana, S.; Dehaini, D.; Nguyen, P.; Angsantikul, P.; Wen, C.H.; Kroll, A.V.; Carpenter, C.; Ramesh, M.; Qu, V.; Patel, S. H.; Zhu, J.; Shi, W.; Hofman, F. M.; Chen, T. C.; Gao, W. W.; Zhang, K.; Chien, S.; Zhang, L. F. *Nature* **2015**, 526, 118-121.
(26) Gao, W.; Hu, C.-M.J.; Fang, R.H.; Luk, B.T.; Su, J.; Zhang, L. *Adv. Mater.* **2013**, 25, 3549-3553.
(27) Aryal, S.; Hu, C.-M.J.; Fang, R.H.; Dehaini, D.; Carpenter, C.; Zhang, D.-E.; Zhang, L. *Nanomedicine* **2013**, 8, 1271-1280.
(28) Fang, R.H.; Hu, C.-M.J.; Luk, B.T.; Gao, W.; Copp, J.A.; Tai, Y.; O'Connor, D.E.; Zhang, L. *Nano Lett.* **2014**, 14, 2181-2188.
(29) Han, K.; Lei, Q.; Jia, H.-Z.; Wang, S.-B.; Yin, W.-N.; Chen, W.-H.; Cheng, S.-X.; Zhang, X.-Z. *Adv. Funct. Mater.* **2015**, 25, 1248-1257.
(30) Lin, Y.-S.; Wu, S.-H.; Tseng, C.-T.; Hung, Y.; Chang, C.; Mou, C.-Y. *Chem. Commun.* **2009**, 3542-3544.
(31) Tang, F.Q.; Li, L.L.; Chen, D. *Adv. Mater.* **2012**, 24, 1504-1534.
(32) Li, L. L.; Guan, Y. Q.; Liu, H. Y.; Hao, N. J.; Liu, T. L.; Meng, X. W.; Fu, C. H.; Li, Y. Z.; Qu, Q. L.; Zhang, Y. G.; Ji, S. Y.; Chen, L.; Chen, D.; Tang, F. Q. *Acs Nano* **2011**, 5, 7462-7470.
(33) Liu, F.; Chen, Y.F.; Liang, Y.J.; Pan, Z.W. *Opt. Lett.* **2016**, 41, 954-957.
(34) Hu, Q.-J.; Lu, Y.-C.; Yang, C.-X.; Yan, X.-P. *Chem. Commun.* **2016**, 52, 5470-5473.
(35) Luo, D.; Carter, K.A.; Miranda, D.; Lovell, J.F. *Adv. Sci.* **2016**, 1600106.

for TOC only

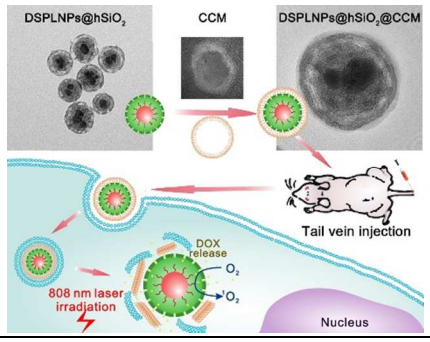
DSPLNPs@hSiO2
CCM
DSPLNPs@hSiO2@CCM
Tail vein injection
DOX release
O2
1O2
808 nm laser irradiation
Nucleus